Accepted Manuscript

Effects of Al addition on the structure and mechanical properties of Zn alloys

Zhilin Liu, Riqing Li, Ripeng Jiang, Xiaoqian Li, Mingxing Zhang

PII: S0925-8388(16)31919-3

DOI: 10.1016/j.jallcom.2016.06.196

Reference: JALCOM 38065

To appear in: *Journal of Alloys and Compounds*

Received Date: 23 April 2016

Revised Date: 9 June 2016

Accepted Date: 21 June 2016

Please cite this article as: Z. Liu, R. Li, R. Jiang, X. Li, M. Zhang, Effects of Al addition on the structure and mechanical properties of Zn alloys, *Journal of Alloys and Compounds* (2016), doi: 10.1016/j.jallcom.2016.06.196.

Effects of Al addition on the structure and mechanical properties of Zn alloys

Zhilin Liu[1, 2]*, Riqing Li[1, 2], Ripeng Jiang[1, 3], Xiaoqian Li[1, 2, 3], Mingxing Zhang[4]*

1. *State Key Laboratory of High-performance Complex Manufacture, Central South University, Changsha, 410083, P.R. China*
2. *College of Mechanical and Electrical Engineering, Central South University, Changsha, 410083, P.R. China*
3. *Light Alloy Research Institute, Central South University, Changsha, 410083, P.R. China*
4. *School of Mechanical and Mining Engineering, The University of Queensland, Brisbane, QLD 4072, Australia*

*Corresponding author: zhilin.liu@csu.edu.cn; mingxing.zhang@uq.edu.au

Abstract

The noticeable improvement of hardness, elongation and yield stress in the cast zinc alloys was achieved using aluminium inoculation. Through varying the addition level of this eutectic-forming solute, the mechanism of such property improvement of cast Zn alloys was investigated. The increase of hardness, elongation and yield stress was very sensitive to the aluminium content due to grain-refinement and solid-solution strengthening. Beyond the maximum solubility of aluminium in zinc, a three-dimensional eutectic network was developed to form a “eutectic-skeleton”, which produced further reinforcement in yield stress and elongation, but only marginal enhancement in hardness. These improved mechanical properties are found to be closely associated with significant microstructural refinement. The microstructural refinement, i.e. the columnar-to-equiaxed transition and the reduction in grain sizes, was mainly elucidated in terms of the Interdependence theory.

Key words: Zn-Al alloys; Microstructure; Mechanical properties; Grain refinement; Interdependence theory

1. Introduction

Zinc alloys have attractive combination of properties, i.e. low melting temperature, good damping properties, sound dimensional tolerance, and excellent corrosion resistance [1-8]. Normally, Zn alloys are used in electronic, coating, transportation and construction industries [1-4]. However, the application of Zn alloys is astricted because of their low strength and brittle fracture, which is mainly caused by the coarse-grained HCP microstructures in cast Zn alloys [6, 11]. Using grain refinement technique, most coarse-grained metals/alloys (i.e. Al,

Mg, Ti and their alloys) can be transformed into the polycrystalline metallic materials with a fine, equiaxed and uniform grain structure. Normally, such microstructural transformation delivers enhanced mechanical properties, consequently promoting follow-up plastic processing [10].

Previous work [11-14] on cast Al and Mg alloys verified the essential contribution of peritectic reaction/nucleation in grain refinement. For instance, the as-cast grain sizes of Al and Mg can be efficiently reduced through addition of Ti and Zr into liquid Al and Mg, respectively. Wang et al. reported that inoculation of peritectic-forming elements, i.e., V, Zr and Nb, efficiently grain refined the as-cast pure Al. However, the grain refining efficiency of eutectic-forming elements, i.e., Mg, Cu and Si, is very marginal. Thus, it was proposed that peritectic reaction is important, even essential, in the grain refinement of cast Al. But, it has still not been fully verified whether the previously established grain refinement theories/models in light metals/alloys, i.e., Al and Mg, can be directly used to cast Zn alloys. Recently, the significant grain refinement of cast Zn was obtained through peritectic-forming elements' (Cu and/or Ag) inoculation [14, 15]. However, as both Cu and Ag have much higher melting temperatures than Zn, it is not cost and economically effective using Cu or Ag as grain refiner for Zn alloy. According to the phase diagrams [16, 17], Cu and/or Ag are peritectic-forming elements. The grain refinement of cast Zn through Cu (or Ag) inoculation was mainly attributed to the enhanced *in-situ* heterogeneous nucleation [14, 15]. However, the maximum grain refining efficiency in such Zn-Cu (or Zn-Ag) peritectic alloys was only achieved when the addition of Cu (or Ag) reached over 2.0 wt.% Cu (or 3.5 wt.% Ag). Moreover, the inactive pro-peritectic intermetallic compounds ($AgZn_3$ or $CuZn_4$) are quite large and brittle, which severely impairs both strength and ductility of cast Zn alloys. Therefore, it is necessary to find an alternative approach to reinforce the mechanical properties of cast Zn alloys.

In the present work, the microstructural modification of cast Zn alloys was obtained through adding the eutectic-forming Al element. The mechanical properties, i.e. yield strength, hardness and elongation, were found to be improved. However, a couple of fundamental questions still remain unclear: (1) what are the primary strengthening components that contribute to the improved mechanical properties? (2) what is the quantitative relationship between microstructural factors (i.e. grain size and solute content) and yield strength in the grain-refined Zn-Al alloys? (3) whether the peritectic-forming solute is essential for grain refinement of cast Zn alloys? (4) what are the specific roles of eutectic-

forming Al solute on the microstructural modification of cast Zn alloys? The present work aims to address all these questions.

2. Experimental

2.1. Materials and casting process

To examine the role of eutectic-forming Al on the microstructural modification of cast Zn, five binary Zn alloys nominally containing 0.25%, 0.50%, 1.00%, 1.50% and 2.00 wt.% Al were accordingly made at 600 ^{o}C. Hereinafter, all compositional contents are expressed in wt.% unless specified otherwise. The Al was added into the pure Zn in the form of master alloys. The master alloy, Zn-6.0wt.% Al, was prepared in a clay-bonded and boron nitride coated graphite crucible by melting the super-high-purity zinc ingots (99.995% pure) and aluminium pellets (99.95% pure) at 700 ^{o}C in an induction furnace with the protection of argon atmosphere. The Zn-Al binary alloys were produced in an electrical resistance furnace also using the same graphite crucible. After melting of pure Zn at 600°C and various amount of Al was added, the melts were isothermally inoculated for 20 minutes, followed by dross cleaning and stirring. Then, the melts were cast into the cylindrical graphite moulds that had been preheated at 600°C. The moulds were 30 mm in diameter and 180 mm in length with a wall thickness of 10 mm. During cooling in air, the moulds were placed on and covered by fiberfrax boards. Details of the cooling method can be found elsewhere [18]. The chemical compositions were determined by inductively coupled plasma atomic emission spectroscopy (ICP-AES). The nominal and actual composition, of the master alloy and the five Zn-Al alloys, are listed in Table 1. The actual Al contents in the alloys are lower than the nominal content. For the purpose of convenience, in the present work, the nominal contents are used to represent the alloys.

2.2. Mechanical properties' examination

In a stable electrical resistance furnace, the as-cast cylindrical Zn-Al ingots were homogeneously annealed at 340 ^{o}C for 3 hours. At this temperature, the solid solubility of Al in Zn is around 1.0 wt.%. Then, these cylindrical ingots were machined into standard tensile samples for tensile test. The tensile samples, with 12.5 mm gauge length and 6.0 mm gauge diameter, are shown in Fig. 1. At a crosshead speed of 0.5 mm/s, the tensile test was completed at room temperature in an INSTRON® testing machine. So as to measure the tensile strain, a pair of extensometers were attached to the tensile samples for strain analysis.

0.2% proof stress was determined and selected as the yield strength. Both yield strength and elongation were obtained based on the average values of three tensile samples that were cut from the same annealed ingots. Small blocks were also cut off from the ingots for hardness test, which was carried out on a Wilson® Tukon™ 1102 machine.

2.3. Microstructural characterization

Metallographic samples were transversely sectioned from middle of the annealed ingots. After mechanically grinding and polishing, each sample was etched in a Gennone-Kersey solution (84% distilled water, 15% H_2SO_4 and 1 vol.% HF), followed by microstructural examination in a Leica® polarised light microscopy (LM). Spot32 image analysis software was equipped on the Leica® LM for grain size measurement. The average grain sizes were measured using a linear intercept technique (ASTM E112-10). Depending on the actual grain size in each field, nine fields were examined and over 60 counts were obtained whenever possible. Using X-ray diffraction (XRD), phase identification of each alloy was accomplished in a Bruker D8 diffractometer. XRD was operated at 40 kV with Cu-K_α radiation (wavelengths $\lambda_{k\alpha1}$ = 1.54056 Å). Further, the detailed information, i.e. microstructure and fracture, was revealed by scanning electron microscopy (SEM; JEOL 7001) equipped with energy dispersive X-ray spectroscopy (EDS). Evolution of crystallographic orientation, i.e. Euler space, angle deviation and crystal structure, were characterized using electron backscattering diffraction (EBSD). The EBSD detector, combined with an Oxford Instrument AZtecHKL® system, was installed on SEM JEOL 7001.

3. Results

3.1. Improved mechanical properties against Al contents

Representative engineering stress-strain curves of each alloy are shown in Fig. 1. It can be seen that both the strength and ductility are concurrently increased with increasing Al contents. On the stress-strain curves, the visible onset of necking region occurred in the Zn-1.5 wt.% Al and Zn-2.0 wt.% Al alloys, which indicates a higher elongation, as shown in Fig. 1. The elongation of pure Zn, Zn-0.25% Al, Zn-0.50% Al, Zn-1.00% Al, Zn-1.50% Al and Zn-2.00wt.% Al were measured to be 0.2, 0.5, 2.5, 3.0, 8.0 and 12 %, respectively (see Fig. 2(a)). This result illustrate a very strong dependence of elongation on Al contents. Moreover, the average hardness of pure Zn, Zn-0.25% Al, Zn-0.50% Al, Zn-1.00% Al, Zn-1.50% Al and Zn-2.00wt.% Al were determined to be 32.5, 43, 55.5, 67, 85 and 91 Hv, respectively, as

indicated in Fig. 2(b). The results show that there is certain relationship between the improved mechanical properties and the Al inoculation, which will be discussed in section 4.

3.2. Fracture analysis and phase identification

After tensile tests, the fracture surfaces of all binary Zn-Al alloys were examined in a SEM. The fractographic images show that a primarily brittle mode of fracture (when Al content is below 0.25 wt.%) was gradually transformed into quasi-ductile fracture (when Al content is over 0.5 wt.%), as shown in Fig. 3. The quasi-ductile fracture appeared in a combined form of brittle and ductile. In other words, the cast Zn-Al alloys that have HCP crystal structure possessed a dominant brittle fracture but with some ductile fracture at high Al contents. Normally, the HCP metals have insufficient slip systems, resulting in a cleavage fracture surface. Compared with the coarse-grained HCP structures of pure Zn in Fig. 3(a), the grain-refined alloys showed some ductile features as shown in Figs. 3(c)-(f). Actually, it has been already documented that the primary brittle fracture of binary cast Zn alloys were hard to be changed only through grain refinement [18].

3.3. Columnar-to-equiaxed transition induced by aluminium

The typical microstructures of the as-annealed binary Zn-Al alloys are shown in Fig. 4. Addition of 0.25 wt.% Al fully converted the predominant columnar grains of pure Zn into equiaxed grains even though the 0.25 wt.% is far below its maximum solubility (C_m = 1.00 wt.% at 340 ^{o}C [19]). The variation of average grain size (d) of the binary Zn-Al alloys with Al contents are plotted in Fig. 5. The present microstructural analysis verified that the difference in the grain sizes before and after annealing at 340°C for 3 hours is ignorable. Thus, it can be seen that the average grain size was reduced from 1878 µm for the pure Zn to 100 µm for the Zn-1.0wt% Al alloy. The grain size of pure Zn was measured by averaging the length and width of columnar grains. Further increase of the Al contents over 1.00 wt.% led to very marginal decrease in the d values. Furthermore, once the grains were refined, the distribution of grain sizes was narrowed as shown by the inset in Fig. 5. The significant grain refinement was achieved at an addition level of 1.0 wt.% Al, where the d value decreased to ~ 100 µm. Fig. 6 shows the difference of the grain boundary orientations before and after Al inoculation. After Al inoculation, the preferential growth direction of pure Zn become randomly-distributed in the Euler space. Meanwhile, the density of Euler angles is largely increased, which addresses grain refinement from a perspective of crystallography.

4. Discussion

4.1. Strengthening through grain refinement and solid solution

It is well recognized that most metals/alloys can be strengthened by single or combined mechanisms. These include grain refinement [20, 21], precipitation [22, 23], particle dispersion [24], solid solution [24, 26], strain/work hardening [27, 31] and etc. Extensive studies on the strengthening mechanisms have been conducted in Al and Al alloys [29, 30], Mg and Mg alloys [23, 31-34], steels [35] and etc. Normally, it is hard to distinguish one specific strengthening component from another. Recently, Liu et al established an empirical relationship between yield strength (σ_y), grain size (d), solute content (c) and intrinsic friction (σ_o) in cast Zn alloys [18]. Meanwhile, the individual contribution of grain-refinement and solid-solution strengthening to the overall σ_y value was identified and quantified [18]. In the present binary Zn-Al alloys, the strengthening components, contributing to the improved σ_y, can be individually classified into grain-refinement, solid-solution and the secondary phase strengthening (the eutectic-skeleton), as shown in Fig. 7. The eutectic-skeleton strengthening occurs while the Al addition level is over its maximum solubility.

When the addition of eutectic-forming Al solute is below the maximum solubility (around 1.0 wt.% Al at 340 ^{o}C), there are only solid-solution strengthening and grain-refinement strengthening. Hence, the combined effects can be expressed using the following equation [36].

$$\sigma_{y1} = \sigma_o + k_{ss}c^{n} + k_{H\text{-}P}d^{-1/2} \quad (1)$$

where σ_{y1} (MPa) is the experimental yield strength, k_{ss} (MPa·(at.)$^{-n}$) is a fitting coefficient, c is the solute content in at.%, n is determined to be 0.52 [18], $k_{H\text{-}P}$ (MPa·m$^{1/2}$) is termed as the Hall-Petch coefficient, and d is the average grain size. Regarding the cast dilute Zn-Al alloys, our previous investigation shows that Eq. (1) is determined as Eq. (2) [18].

$$\sigma_{y1} = 11.02 + 83.6c^{0.52} + 0.56d^{-1/2} \quad (2)$$

When Al content was ≥ 1.0 wt.%, the three-dimensional (3-D) η-Zn/(Al) eutectic network developed to form an “eutectic-skeleton”. Through careful SEM examination, it was found to be the η-Zn/(Al) eutectic-skeleton, as shown in Fig. 8(a). Fig. 8(a) indicates that these η-Zn/(Al) eutectic structure, between any two adjacent η-Zn grains, was connected to each other, forming the η-Zn/(Al) eutectic-skeleton in 3-D space. Moreover, the eutectic-forming

Al solute mainly distributed along grain boundaries (see Fig. 8(b)). Such 3-D eutectic-skeleton will contribute to the alloys' strength [37]. Thus, an extra strengthening component (eutectic-skeleton) should be taken into account when the Al content is over 1.0 wt.%. Further, the combined strengthening components are arranged as Eq. (3).

$$\sigma_{y2} = \sigma_o + k_{ss}c^n + k_{H\text{-}P}d^{-1/2} + \sigma_{es} \quad (3)$$

in which σ_{y1} (MPa) is the experimental yield strength, σ_{es} (MPa) is the strengthening component from the 3-D eutectic-skeleton, and other parameters can be found in Eq. (1). The experimentally-determined yield stress (σ_{y2}) was plotted as a function of Al contents, as shown in Fig. 9. The difference between experimental results (σ_{y2}) and theoretical prediction (σ_{y1}) occurred for the alloy with over 1.0wt% Al, which implies an unknown strengthening component (highlighted by the inset in Fig. 9). This unknown strengthening component should be resulted from the 3-D eutectic-skeleton. Based on Eq. (2) and experimental results, the theoretical prediction quantifies the contributions from grain-refinement and solid-solution. The σ_{es} values of Zn-1.5wt.% Al and Zn-2.0wt.% Al were calculated to be ~ 8 and 18 MPa, respectively. In other words, the 3-D eutectic-skeleton contributed ~ 8 and 18 MPa to the overall σ_{y2} of binary Zn-1.5wt.% Al and Zn-2.0wt.% Al alloys, respectively. This is equivalent to a value comparable to the grain-refinement strengthening for a virtual grain size of ~ 80 μm.

4.2. Microstructural evolution and associated grain-refining mechanism

The grain refinement has twofold, i.e. the columnar-to-equiaxed transition (CET) and the reduction of equiaxed grain size [14, 38]. The variation of the average grain size (d) of Zn-Al alloys with Al contents are plotted in Fig. 5. This trend of experimental result agrees well with our previous report in the eutectic Zn-Mg alloys [10]. However, it differs from the results of eutectic binary Al alloys (Al-Cu, Al-Mn and Al-Si) reported by Wang et al [13]. In their eutectic binary Al alloys, noticeable CET cannot be generated, even though the addition levels were over their respective C_m. Modelling of grain refinement at a microscopic scale is generally classified into two categories including deterministic- and probabilistic approaches [39, 40]. A couple of analytical and/or predictive models have been developed to assess the dependence of d values on the relevant factors. Recently, StJohn et al studied the grain refinement of Al, Mg, Ti and their alloys, and developed a deterministic approach [41, 42]. According to StJohn et al's approach, the d values of cast metals are quantified as follows:

$$d = \frac{D \cdot z \cdot \Delta T_n}{vQ} + \frac{4.6 \cdot D}{v}\left(\frac{C_l^* - C_o}{C_l^*(1-k)}\right) + x_{sd} \quad (4)$$

In Eq. (4), D, $z \cdot \Delta T_n$, v, Q, C_l^*, C_o, k and x_{sd} represent the diffusion coefficient, critical constitutional supercooling (CS) required for nucleation, growth velocity, growth restriction factor, solute concentration at solid/liquid (S/L) interface, initial solute concentration in liquid, partition coefficient and interparticle spacing, respectively. Eq. (4) is also termed as "Interdependence theory". In the Interdependence theory, both potent nucleant particles and solute additions are considered as essential factors that contribute to grain refinement [43-44]. Q is defined by $d(\Delta T_c)/df_s|_{fs=0}$, where ΔT_c and f_s are CS and solid fraction, respectively. In a binary alloy system, Q equals to $mc_o(k\text{-}1)$, in which m is the slope of liquidus, and k and c_o can be found in Eq. (4). Based on extensive experiments, Q has been verified to be an effective parameter for quantifying the solute effect on decreasing d [45, 46]. For a given alloy system that is cooled at 1 $^oC/s$, Eq. (4) can be simplified as Eq. (5) for practical application [47].

$$d = a + b/Q \quad (5)$$

Based on present experimental data, the linear quantitative relationship between d and $1/Q$ was derived in Fig. 10, i.e. $d = 78.78 + 265.47/Q$ with a regression coefficient of 0.96. In eutectic Al-Cu, Al-Mg and Al-Si alloy systems, Wang et al reported that the intercept/gradient (a/b) values of the best fitting lines are 926/232, 939/251 and 921/208, respectively [13]. The CET in Al-Cu, Al-Mg and Al-Si are very marginal. The alloy systems, with lower values of a and b, imply a higher grain refining efficiency [41]. Compared with the Al-Cu, Al-Mg and Al-Si eutectic systems, the present Zn-Al system possesses a much lower a value and a comparable b value, which indicates a high grain refining efficiency. According to Interdependence theory, the columnar-to-equiaxed transition (CET) in Zn-Al alloys was mainly governed by Q-value and the heterogeneous nucleation. From a perspective of Zn-Al phase diagram [48], no intermetallic particles should form to serve as the heterogeneous nucleation sites for η-Zn grains. However, the η-Zn grains may still nucleate on either the Al-enriched clusters, (Al) fragments or the native potent particles that are present in melts. Actually, similar phenomenon were also reported in Mg-Al alloy [49] and Al-Si alloy [50]. The Al-enriched clusters, (Al) fragments and the native potent particles may come from master alloy or *in-situ* formation. Such hypothesis is also crystallographically

rational. For instance, three orientation relationships (ORs) have already been verified as follows in binary Zn-Al alloys [51]:

$$[11\bar{2}0]_{\eta-\mathrm{Zn}}||[110]_{(\mathrm{Al})},\ (0002)_{\eta-\mathrm{Zn}}\ 1.10^{o}\ \text{from}\ (\bar{1}11)_{(\mathrm{Al})} \quad (6)$$

$$[11\bar{2}0]_{\eta-\mathrm{Zn}}||[110]_{(\mathrm{Al})},\ (\bar{1}101)_{\eta-\mathrm{Zn}}\ 0.82^{o}\ \text{from}\ (002)_{(\mathrm{Al})} \quad (7)$$

$$[\bar{1}100]_{\eta-\mathrm{Zn}}||[112]_{(\mathrm{Al})},\ (0002)_{\eta-\mathrm{Zn}}\ 4.50^{o}\ \text{from}\ (\bar{1}11)_{(\mathrm{Al})} \quad (8)$$

Each OR corresponds to an energetically-favourable interface between η-Zn and (Al). According to the crystallographic matching theory [52, 53], occurrence of these ORs will enhance the heterogeneous nucleation of η-Zn on (Al) fragments, further leading to grain refinement.

5. Conclusions

Addition of eutectic-forming Al solute to cast Zn resulted in the noticeably-reinforced properties, i.e. hardness, elongation and yield stress. The hardness, elongation and yield stress of cast binary Zn-Al alloys were improved from 0.2%, 32.46 Hv and 17.5 MPa to 12%, 91 Hv and 150 MPa, respectively. These improved properties were mainly attributed to grain-refinement, solid-solution and eutectic-skeleton. Once the Zn-Al alloys with over 1.0 wt.% Al were annealed at 340 ^{o}C for 3 hrs, a three-dimensional (3-D) eutectic network was developed to form a 3-D “eutectic-skeleton”. The eutectic-skeleton contributed around 8 and 18 MPa to the overall yield stress of Zn-1.5wt.% Al and Zn-2.0wt.% Al, respectively. Although a very large range of grain sizes (d) was obtained from 1878 to 100 μm, fractographic examination of the deformed tensile samples reproducibly identified a quasi-ductile mode of fracture in the cast Zn-Al alloys. Through the addition of eutectic-forming Al solute into cast pure Zn, the significant columnar-to-equiaxed transition (CET) was obtained. Thus, the peritectic-forming solute is not a prerequisite for microstructural refinement of cast Zn alloys. According to Interdependence theory, the CET is proposed to be mainly resulted from the growth restriction factor (Q) and the potent native nucleant particles. Based on experimental data, a quantitative linear relationship, $d = 78.78 + 265.47/Q$, was derived with a regression coefficient of 0.96.

Acknowledgement

Zhilin Liu would like to appreciate the State Key Laboratory of High-performance Complex Manufacture for funding support (grant No. ZZYJKT2016-03) and the Open-End Fund for the Valuable and Precision Instruments of Central South University. The National Natural Science Foundation of China is also gratefully acknowledged for funding support (grant No. 51475480).

References

[1] A. Green, J. Wesemael, Zinc die casting alloys and sustainability, Die Casting Engineer 03 (2009) 56-58.

[2] D.P.M. Apelian, D.C. Herrschaft, Casting with zinc alloys, J. Met. 33 (1981) 12-20.

[3] J. Marberg, Corrosion resistance of zinc and zinc alloys, Materials and Corrosion 46 (1995) 434-435.

[4] F.M. Azizan, H. Purwanto, M.Y. Mustafa, Effect of adding Ag on tensile and microstructure properties of zinc alloys, Inter. J. Eng. Technol. 12 (2012) 78-84.

[5] A.E. Ares, C.E. Schvezov, The effect of structure on tensile properties of directionally solidified Zn-based alloys, J. Cryst. Growth. 318 (2011) 59-65.

[6] S.F. Gueijman, C.E. Schvezov, A.E. Ares, Vertical and horizontal directional solidification of Zn-Al and Zn-Ag diluted alloys, Mater. Trans. 51 (2010) 1861-1870.

[7] M.R. Rosenberger, A.E. Ares, I.P. Gatti, C.E. Schvezov, Wear resistance of dilute Zn-Al alloys, Wear 268 (2010) 1533-1536.

[8] A.E. Ares, L.M. Gassa, C.E. Schvezov, M.R. Rosenberger, Corrosion and wear resistance of hypoeutectic Zn-Al alloys as a function of structural features, Mater. Chem. Phys. 136 (2012) 394-414.

[9] W.F. Smith, Structure and properties of engineering alloys, second ed., McGraw-Hill College, New York, 1992.

[10] Z. Liu, D. Qiu, W. Feng, J.A. Taylor, M.X. Zhang, Grain refinement of cast zinc through magnesium inoculation: Characterisation and mechanism, Mater. Character. 106 (2015) 1-10.

[11] F.A. Crossley, Grain Refinement by the Peritectic Reaction in Aluminum and Aluminum Base Alloys, Illinois Institute of Technology, 1950.

[12] E.F. Emley, Principles of magnesium technology, Pergamon Press, Oxford, 1966.

[13] F. Wang, Z. Liu, D. Qiu, J.A. Taylor, M.A. Easton, M.X. Zhang, Revisiting the role of peritectics in grain refinement of Al alloys, Acta Mater. 61 (2013) 360-370.

[14] Z. Liu, D. Qiu, W. Feng, J.A. Taylor, M.X. Zhang, The grain refining mechanism of cast zinc through silver inoculation, Acta Mater. 79 (2014) 315-326.

[15] Z. Liu, D. Qiu, W. Feng, J.A. Taylor, M.X. Zhang, Crystallography of grain refinement in cast zinc-copper alloys, J. Appl. Crystal. 48 (2015) 890-900.

[16] P. Villars, Zn-Ag phase diagram, alloy phase diagrams center™, ASM International, OH, 2006.

[17] P. Villars, Zn-Cu phase diagram, alloy phase diagrams center™, ASM International, OH, 2006.

[18] Z. Liu, D. Qiu, F. Wang, J.A. Taylor, M.X. Zhang, Effect of grain refinement on tensile properties of cast zinc alloys, Metall. Mater. Trans. A (2015) 1-12.

[19]Z. Liu, F. Wang, D. Qiu, J.A. Taylor, M.X. Zhang, The effect of solute elements on the grain refinement of cast Zn, Metall. Mater. Trans. A 44 (2013) 4025-4030.

[20] N.J. Petch. J. Iron Steel Inst. (Lond) 174 (1953) 4.

[21] E.O. Hall, The deformation and ageing of mild steel: discussion of results, Proc. Phys. Soc. (Lond) B64 (1951) 6.

[22] D.G. Westlake, Precipitation strengthening in crystals of zirconium-hydrogen alloys containing oxygen as an impurity, Acta Metallurgica 12 (1964) 1373-1380.

[23] J.F. Nie, Precipitation and hardening in magnesium alloys, Metall. Mater. Trans. A 43 (2012) 3891-3939.

[24] J. Rösler, E. Arzt, A new model-based creep equation for dispersion strengthened materials, Acta Metall. Mater. 38 (1990) 671-683.

[25] A. Akhtar, E. Teghtsoonian, Solid solution strengthening of magnesium single crystals-I alloying behaviour in basal slip, Acta Metallurgica 17 (1969) 1339-1349.

[26] Y. Nakada, A.S. Keh, Solid solution strengthening in Fe-N single crystals, Acta Metallurgica 16 (1968) 903-914.

[27] M.C. Shaw, A quantized theory of strain hardening as applied to the cutting of metals, J. Appl. Phys. 21 (1950) 599-606.

[28] N.F. Mott, A theory of work-hardening of metal crystals, Phil. Mag. Series 7/43 (1952) 1151-1178.

[29] K.L. Kendig, D.B. Miracle, Strengthening mechanisms of an Al-Mg-Sc-Zr alloy, Acta Mater. 50 (2002) 4165-4175.

[30] J.S. Hayes, Effect of grain size on tensile behaviour of a submicro grained Al-3wt.%-Mg alloy produced by sever deformation, Mater. Sci. Tech. 16 (2000) 1259-1263.

[31] K. Kubota, M. Mabuchi, K. Higashi, Review processing and mechanical properties of fine-grained magnesium alloys, J. Mater. Sci. 34 (1999) 2255-2262.

[32] D. Qiu, M.X. Zhang, Strengthening mechanisms and their superposition law in an age-hardenable Mg-10wt.% Y Alloy, Metall. Mater. Trans. A 43 (2012) 3314-3324.

[33] J.T. Wang, D.L. Yin, J.Q. Liu, J. Tao, Y.L. Su, X. Zhao, Effect of grain size on mechanical property of Mg–3Al–1Zn alloy, Scripta Mater. 59 (2008) 63-66.

[34] B. Kim, C.H. Park, H.S. Kim, B.S. You, S.S. Park, Grain refinement and improved tensile properties of Mg–3Al–1Zn alloy processed by low-temperature indirect extrusion, Scripta Mater. 76 (2014) 21-24.

[35] K. Muszka，J. Majta，Ł. Bienias, Effect of grain refinement on mechanical properties of microalloyed steels, Metall. Foundary Eng. 32 (2006) 12.

[36] C.H. Cáceres, D.M. Rovera, Solid solution strengthening in concentrated Mg–Al alloys, J. Light Metals 1 (2001) 151-156.

[37] B. Zhang, A.V. Nagasekhar, X. Tao, Y. Ouyang, C.H. Cáceres, M. Easton, Strengthening by the percolating intergranular eutectic in an HPDC Mg–Ce alloy, Mater. Sci. Eng. A 599 (2014) 204-211.

[38] A.L. Greer, P.S. Cooper, M.W. Meredith, W. Schneider, P. Schumacher, J.A. Spittle, A. Tronche, Grain refinement of aluminium alloys by inoculation, Adv. Eng. Mater. 5 (2003) 81-91.

[39] M. Rappaz, C.A. Gandin, Probabilistic modelling of microstructure formation in solidification processes, Acta Metall. Mater. 41 (1993) 345-360.

[40] M. Qian, P. Cao, E.A. Mark, S.D. McDonald, D.H. StJohn, An analytical model for constitutional supercooling-driven grain formation and grain size prediction, Acta Mater. 58 (2010) 3262-3270.

[41] D.H. StJohn, M. Qian, M.A. Easton, P. Cao, The Interdependence theory: the relationship between grain formation and nucleant selection, Acta Mater. 59 (2011) 4907-4921.

[42] M.J. Bermingham, S.D. McDonald, D.H. StJohn, M.S. Dargusch, Beryllium as a grain refiner in titanium alloys, J. Alloys Comp. 481 (2009) 20-23.

[43] M.J. Bermingham, S.D. McDonald, M.S. Dargusch, D.H. StJohn, The mechanism of grain refinement of titanium by silicon, Scripta Mater. 58 (2008) 1050-1053.

[44] A.L. Greer, Grain refinement of alloys by inoculation of melts, Philos. Trans. R. Soc. A Math. Phys. Eng. Sci. 361 (2003) 479-494.

[45] M.A. Easton, D.H. StJohn, A model of grain refinement incorporating alloy constitution and potency of heterogeneous nucleant particles, Acta Mater. 49 (2001) 1867-1878.

[46] P. Desnain, Y. Fautrelle, J.L. Meyer, J.P. Riquet, F. Durand, Prediction of equiaxed grain density in multicomponent alloys, Acta Metall. Materi. 38 (1990) 1513-1523.

[47] M.A. Easton, D.H. StJohn, An analysis of the relationship between grain size, solute content, and the potency and number density of nucleant particles, Metall. Mater. Trans. A 36 (2005) 1911-1920.

[48] H. Baker, H. Okamoto, ASM Handbook: Volume 03-alloy phase diagrams, ASM International, OH, 1992.

[49] P. Cao, M. Qian, D.H. StJohn, Native grain refinement of magnesium alloys, Scripta Mater. 53 (2005) 841-844.

[50] Y. Zhang, H. Zheng, Y. Liu, L. Shi, R. Xu, X. Tian, Cluster-assisted nucleation of silicon phase in hypoeutectic Al–Si alloy with further inoculation, Acta Mater. 70 (2014) 162-173.

[51] M.X. Zhang, P.M. Kelly, Understanding the crystallography of the eutectoid microstructure in a Zn–Al alloy using the edge-to-edge matching model, Scripta Mater. 55 (2006) 577-580.

[52] M.X. Zhang, P.M. Kelly, M.A. Easton, J.A. Taylor, Crystallographic study of grain refinement in aluminum alloys using the edge-to-edge matching model, Acta Mater. 53 (2005) 1427-1438.

[53] M.X. Zhang, P.M. Kelly, Edge-to-edge matching and its applications: Part I. application to the simple HCP/BCC system, Acta Mater. 53 (2005) 1073-1084.

Table (1 table in total)

Table 1 Chemical compositions of major solute elements in the as-cast master alloys, and the nominal and determined Al contents of five binary Zn-Al alloys

Master alloy Zn-6.0wt.% Al	Solute contents in wt.% determined using ICP-AES										
	Zn	Cu	Al	Mg	Fe	Ni	Sn	Mn	Cr	Pb	Cd
	.Bal	.002	5.82±0.10	.001	.003	.001	.002	.001	.001	.001	.001
	Sample group No.			Nominal addition				Determined content			
Binary Zn-Al tensile alloys	1			0.25 Al				0.26 Al			
	2			0.50 Al				0.45 Al			
	3			1.00 Al				0.93 Al			
	4			1.50 Al				1.32 Al			
	5			2.00 Al				1.85 Al			

Figure captions (11 figure captions in total)

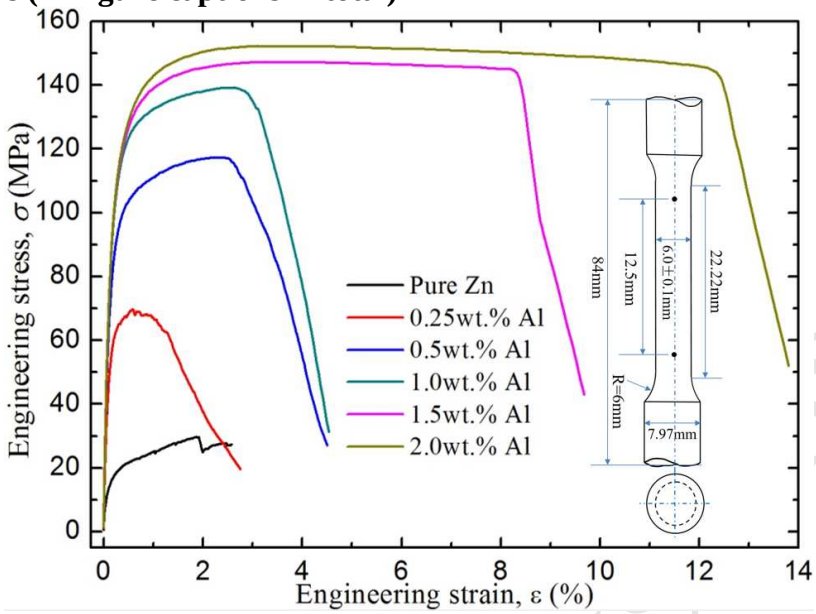

Fig. 1. Representative engineering stress-strain curves of the as-annealed Zn-Al binary alloys. The data for pure Zn in this paper comes from that in Ref. [18].

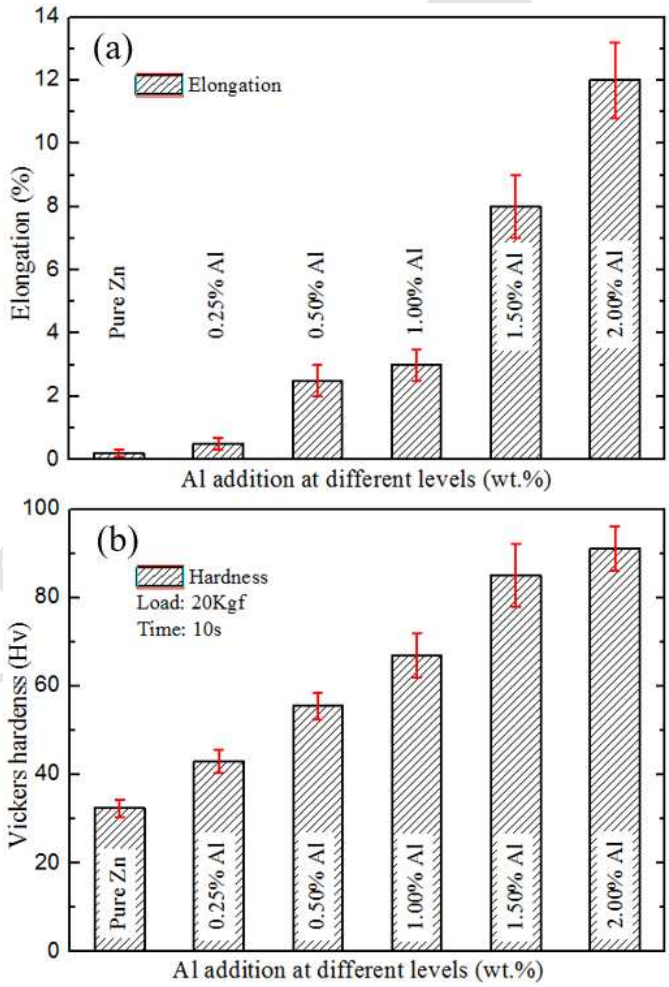

Fig. 2. Variation of (a) elongation and (b) hardness with the eutectic-forming Al contents of the annealed Zn-Al alloys.

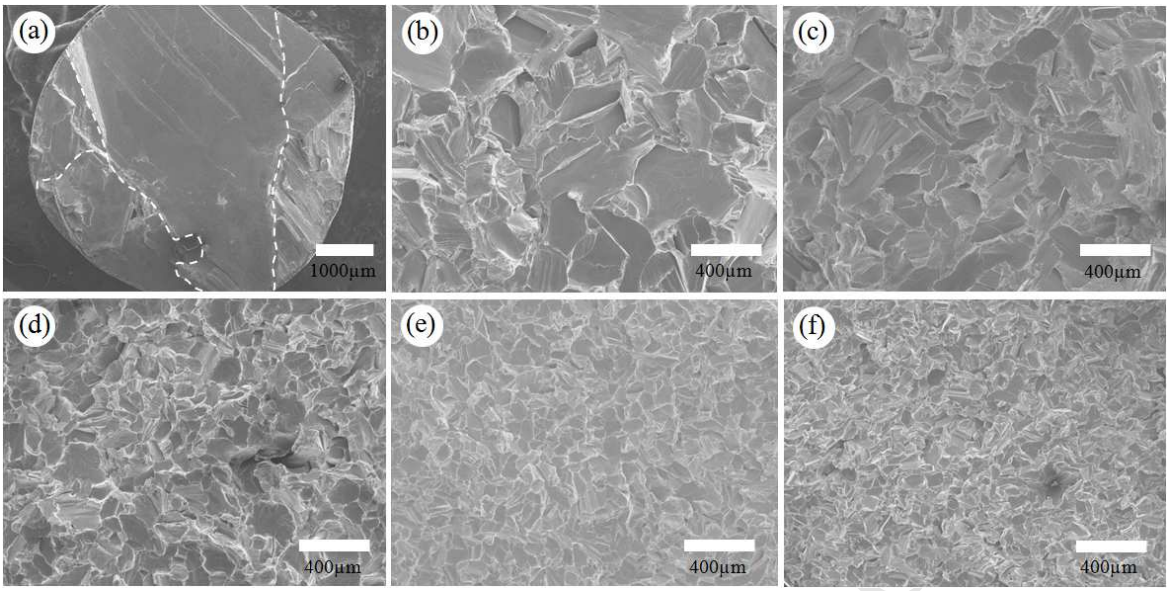

Fig. 3. Tensile fracture of the Zn alloys with different Al contents (in wt.%): (a) pure Zn; (b) Zn-0.25% Al; (c) Zn-0.5% Al; (d) Zn-1.0% Al; (e) Zn-1.5% Al; (f) Zn-2.0% Al. The grain boundaries of pure Zn in (a) are highlighted using white dashed lines, indicating four individual grains.

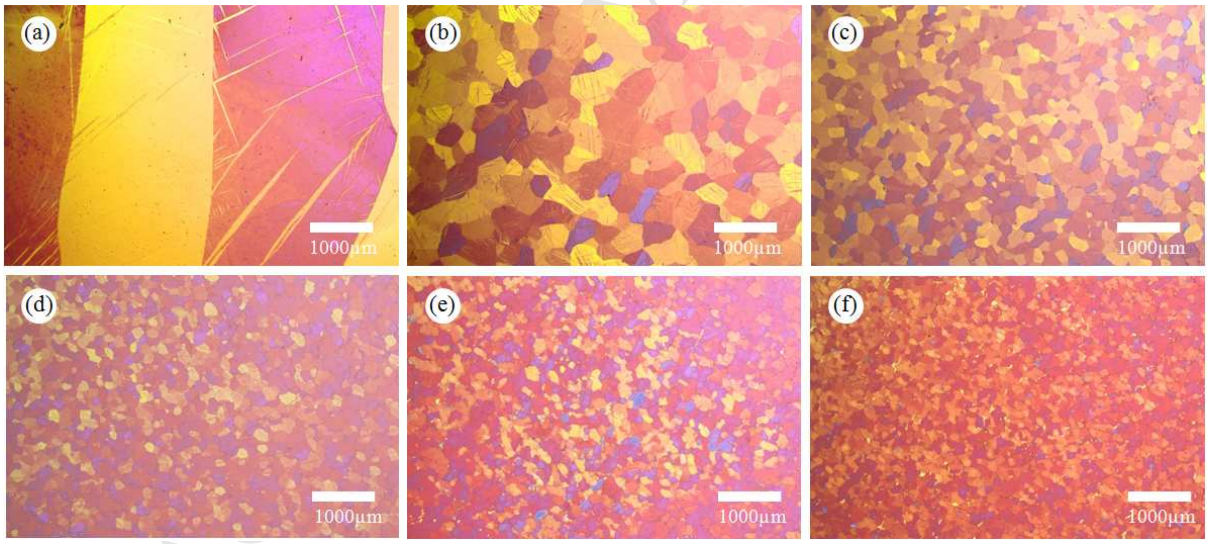

Fig. 4. Representative optical microstructures of the Zn alloys with different amounts of Al addition (in wt.%): (a) pure Zn; (b) Zn-0.25% Al; (c) Zn-0.5% Al; (d) Zn-1.0% Al; (e) Zn-1.5% Al; (f) Zn-2.0% Al.

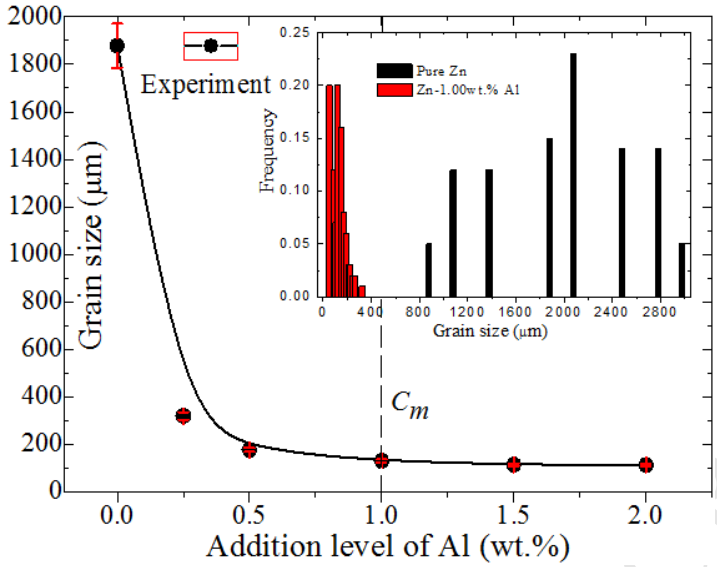

Fig. 5. Measured grain sizes of Zn Alloys plotted against Al contents. Inset histogram indicates the difference of the grain size distribution between pure Zn and Zn-1.00wt.% Al alloy. C_m is the maximum solubility (1.00 wt.%) at 340 ^{o}C.

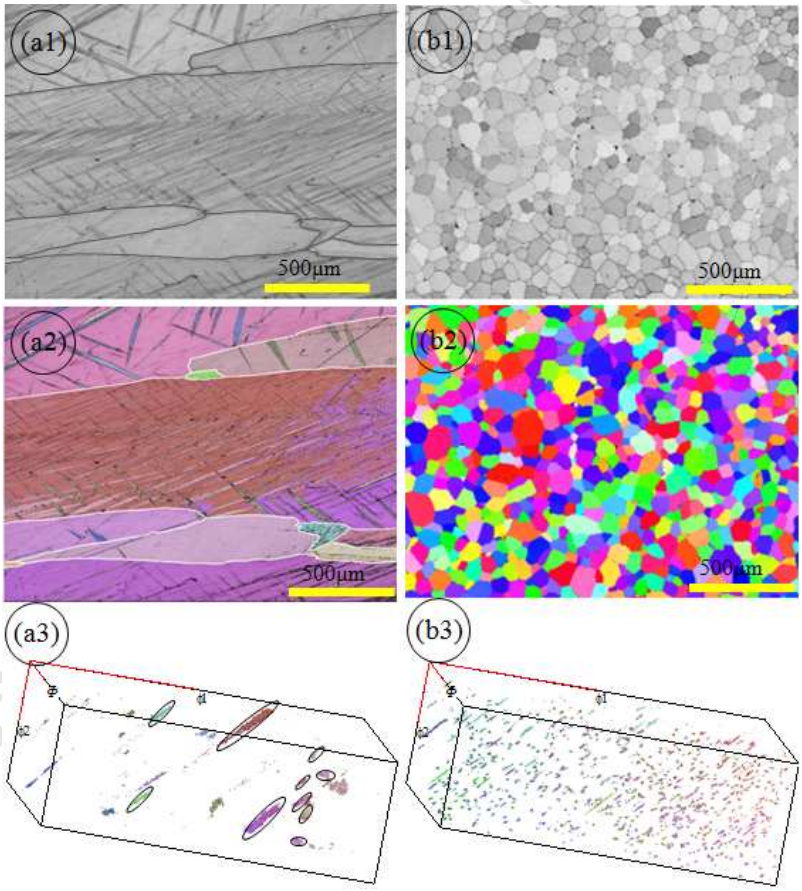

Fig. 6. Difference in the grain boundary orientations between (a) pure Zn [18] and (b) Zn-1.0wt.% Al. (a1) and (b1) are EBSD band contrast, (a2) and (b2) are EBSD orientation mapping, and (a3) and (b3) are Euler space.

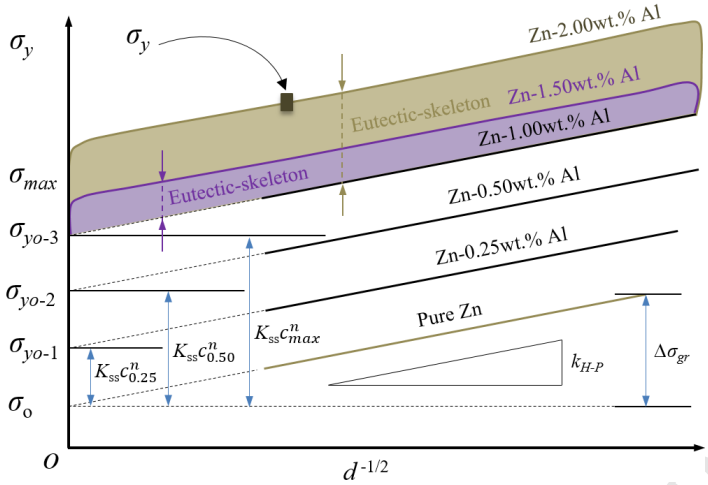

Fig. 7. Schematic illustration of the contributions of different strengthening components in the present binary Zn-Al alloys, including grain-refinement, solid-solution and eutectic-skeleton. σ_y is the experimentally determined yield strength, k_{ss} represents a fitting coefficient, c is the solute content in at.%, σ_o is the intrinsic friction stress, and σ_{gr} is the yield stress by grain refinement.

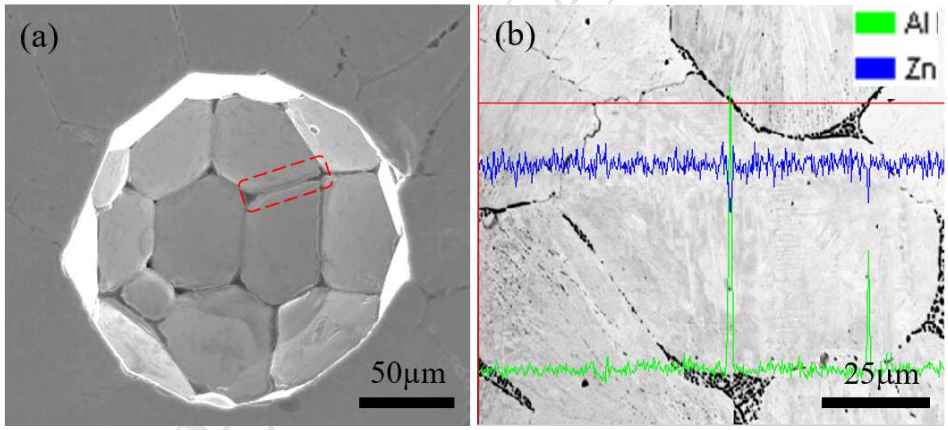

Fig. 8. (a) A representative BSE image of eutectic-skeleton with three-dimensional morphology (red dashed rectangle), and (b) Distribution of eutectic-skeleton at the grain boundaries with two-dimensional morphology. The blue and green curve represent the compositional distribution of Zn and Al along the horizontal red solid line in (b).

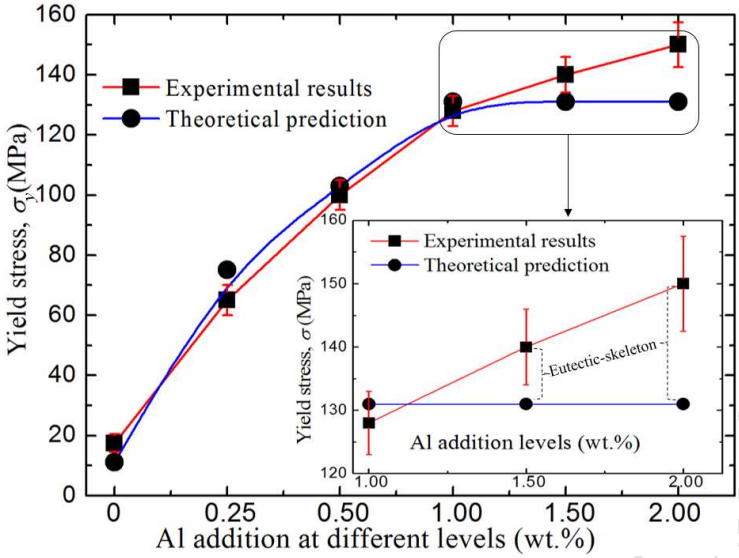

Fig. 9. Difference in yield strength between the experimental results and the theoretical prediction, indicating the eutectic-skeleton strengthening components (highlighted by the inset).

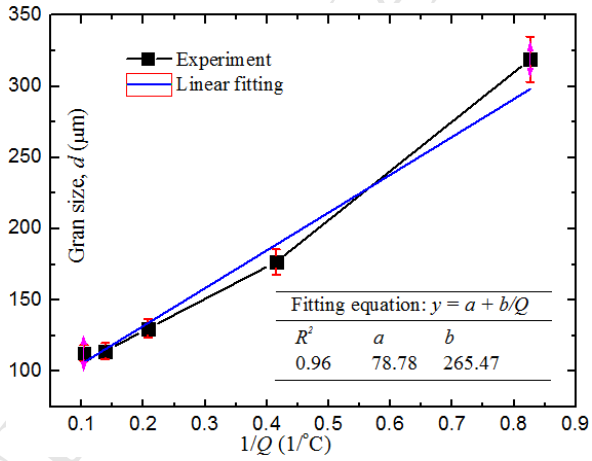

Fig. 10. The quantitative relationship between the average grain sizes (d) of binary Zn-Al alloys and the inverse of growth restriction factor ($1/Q$). The contents of eutectic-forming Al solute in the binary Zn-Al alloys range from 0.25 to 2.0 wt.%. Regression coefficient (R^2) and fitting equation ($y = a + b/Q$) are imposed on this figure.

23 June 2016

Central South University

Changsha, Hunan

P.R. China

To

The Editor/Reviewer

Journal of Alloys and Compounds

Highlights

- Hardness, elongation and yield stress of Zn-Al alloys were significantly improved.
- Remarkable columnar-to-equiaxed transition was generated by eutectic-forming Al.
- Contribution of a 3-D “eutectic-skeleton” to the final yield stress was quantified.
- Relationship, between microstructure and improved properties, was investigated.
- Peritectic-forming solute is proved unnecessary for grain refinement of Zn alloys.